Lecture 4 — Wave and particle beams.

1 Introduction

In the previous lectures, we have learned about the classification of periodic structures based on their symmetry, and we have seen some examples of real crystal structures build out of molecules or atomic frameworks. In this lecture, we will introduce some elements of the theory of scattering of electromagnetic radiation (X-rays) and of particle beams (electrons, neutrons), which are all essential tools to analyse the atomic structure of real crystals. In this course, we will be primarily concerned with *elastic scattering* (diffraction), which can determine the following properties of crystalline matter:

- **The crystal structure**, i.e., the position of the atoms in the crystal *averaged* over a large number of unit cells and over time. This information is extracted from Bragg diffraction, i.e., from the sharp diffraction spots that are the characteristic feature of crystal diffraction. As we have seen, sharp spots centred at the reciprocal lattice points arise as a consequence of real-space periodicity (i.e., regardless of the detailed structure or even of the atomicity of the crystal) in the process of calculating a 3-dimensional Fourier transform of a lattice function. Bragg diffraction is observed for X-ray, neutron and electron scattering, although, for the latter technique, it is less straightforward to obtain quantive crystal structure information.

- **The deviation from perfect periodicity**. No real crystal structure has perfect, infinite translational order, if nothing else, because all real crystals have a finite size and all atoms are subject to thermal motion (at zero temperature, to *zero-point motion*). The general consequence of these deviations from perfect periodicity is that the scattering will no longer occur exactly at the RL points (δ functions), but will be "spread out". Finite-size effects and metric fluctuation of the size of the unit cell (known as *strain* — often due to the presence of *stresses* in the crystal), produce *peak broadening* without altering the integrated cross section (amount of "scattering power") of the Bragg peaks. These "peak broadening" effects are of course convoluted with the instrumental resolution of the probe being employed. Fluctuation in the atomic positions (e.g., due to thermal motion) or in the scattering amplitude of the individual atomic sites (e.g., due to substitutions of one atomic species with another), give rise to a selective reduction of the intensity of certain Bragg peaks by the so-called *Debye-Waller factor*, and to the appearance of intensity elsewhere in reciprocal space (*diffuse scattering*). Analysis of peak widths, Debye-Waller factors and of diffuse scattering can be employed to extract information about crystal defects, particle sizes, internal stresses and thermal motion.

- **The case of liquids and glasses**. Here, crystalline order is absent, and so are Bragg diffraction peaks, so that all the scattering is "diffuse". Nonetheless, scattering of X-rays and neutrons from liquids and glasses is exploited to extract *radial distribution functions* — in essence, the probability of finding a certain atomic species at a given distance from another species. This information, together with previous knowledge of the molecular structure of the liquid or of the stable atomic clusters in a complex glass, often enables one to paint very detailed pictures of the structure of disordered materials.

- **The magnetic structure**. Neutron possess a dipole moment and are strongly affected by the presence of internal magnetic fields in the crystals, generated by the magnetic moments of unpaired electrons. Magnetic scattering of X-rays is much weaker, but modern synnchrotron techniques have turned it into a very powerful tool, highly complementary to neutron scattering. As in the case of atomic structures, *ordered* magnetic structures of ferromagnets or antiferromagnets give rise to Bragg scattering, whereas *disordered* magnetic structures (as for paramagnets or "spin glasses" produce magnetic diffuse scattering.

It is important to stress that, in order to extract information about the *atomic* structure of a crystal, liquid or glass by diffraction, **the wavelength of the probe must be comparable or smaller than the interatomic distances**, which are typically a few Ångstroms (10^{-10} m, or 10^{-1} nm). Tab. 1 illustrates the typical wavelengths and energies employed for X-ray, neutron and electron diffraction.

Table 1: Typical wavelenghts and energies employed for X-ray, neutron and electron diffraction. For electromagnetic radiation, $E = hc/\lambda$, with $hc = 12.4$ KeV $\cdot$ Å; for a non-relativistic particle beam, $E = \frac{2\pi^2\hbar^2}{m\lambda^2}$ =, where $\frac{2\pi^2\hbar^2}{m} = 82$ meV $\cdot$ Å^2 for neutrons and 150 eV $\cdot$ Å^2 for electrons. A typical Transmission Electron Microscope (TEM) can operate at 200 KV raising the electron velocity to 70 % of the speed of light, and some state-of-the-art microscopes can reach the MV range; therefore, relativistic effects need to be taken into account in converting between energy and wavelength.

	λ	E
X-rays	0.1–6 Å	2–150 KeV
neutrons	0.3–10 Å	1–1000 meV
electrons	0.02–3 Å	20 eV–200 KeV

Note here that, whereas the wavelength ranges of the different probes are overlapping, the energy ranges are very different — namely are much lower for neutrons than for the other probes. We will return on the subject later on.

In this lecture, we will introduce the interaction of radiation and particle beams with matter, with the goal of understanding how this can be exploited to study the solid state. We will examine in some detail the *interaction between X-rays and matter*, whilst providing only a qualitative description of the of electron- and neutron-matter interaction. We will also learn about the main method of production of these types of radiation.

2 Thomson scattering of X-rays

Bragg diffraction of X-rays is primarily due to the scattering of X-ray from electrons bound to the atoms of the crystal structure. It is generally a very good approximation (we will look at *caveats* and exception later on) to employ the so-called Thomson formula (from J.J. Thomson, Nobel Prize 1906) to calculate the relevant scattering amplitudes and cross sections. This is a bit of a paradox, since the Thomson formula assumes *free* electrons, but the agreement with experiments in nonetheless very good.

2.1 Scattering from a free electron

Thomson scattering is a *classical* phenomenon, and can be explained as follows: as electromagnetic radiation impinges on a free electron, the oscillating electric field subjects it to an acceleration. The scattered radiation is the radiation emitted by the accelerated charge. If a charge is accelerated and is observed in a reference frame where its velocity is *small compared to that of light*, the electric field can be written as

$$\mathbf{E}(\boldsymbol{R}, t) = \frac{(-e)}{4\pi\epsilon_0 c^2}\left[\frac{\mathbf{n}\times(\mathbf{n}\times\mathbf{a})}{R}\right]_{ret} \tag{1}$$

where **a** is the acceleration and **n** is a **unit vector** along the segment connecting the particle to the observer and pointing towards the latter (fig. 1). The subscript "ret" means "**retarded**" (see below).

Note that if we keep rotating the scattered beam in the direction shown in fig. 1, i.e., in the plane *containing* the incident polarisation, the projection $a_\perp$ will eventually become *zero* at 90°. On the other hand, if we rotated *perpendicular* to the incident polarisation, the projection would obviously stay the same. In a nutshell, this is the essence of the polarisation factor.

Before we discuss eq. 1, it is worth reminding the important vector relation (used also later on in

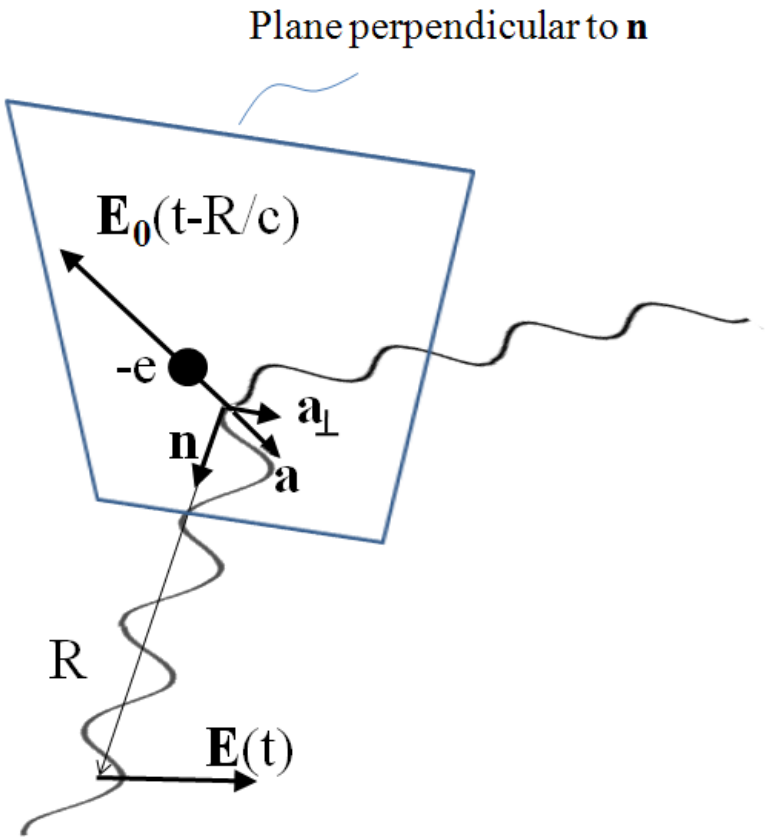

Figure 1: Diagram illustrating the Thomson scattering of X-rays from a free electron. The acceleration due to the incoming wave is $\boldsymbol{a}$, whereas its *projection perpendicular to the line of sight* is $\boldsymbol{a}_\perp$.

the course). For any three vectors:

$$\boxed{\boldsymbol{a} \times (\boldsymbol{b} \times \boldsymbol{c}) = (\boldsymbol{a} \cdot \boldsymbol{c})\boldsymbol{b} - (\boldsymbol{a} \cdot \boldsymbol{b})\boldsymbol{c}} \tag{2}$$

$$\boxed{\mathbf{n} \times (\mathbf{n} \times \mathbf{a}) = -\left[\boldsymbol{a} - (\boldsymbol{a} \cdot \boldsymbol{n})\,\boldsymbol{n}\right]} \tag{3}$$

The expression in square brackets on the right side of eq. 3 is *the projection of $\boldsymbol{a}$ on the plane perpendicular to $\boldsymbol{n}$*

In eq. 1, the square bracket with subscript "ret" means that the quantity in the bracket is to be evaluated at the "retarded" (i.e., **earlier**) time $t - R/c$. R is the distance between the "retarded" position and the observer (fig. 1). Since we are interested in the radiation at a great distance from

the particle and at oscillatory, small-amplitude motions of the latter, we can replace R and $\mathbf{n}$ with constant quantities referring to the average position of the particle.

The electric field due to an accelerated particle is proportional to the *projection of the acceleration perpendicular to the line of sight.*

Let us consider a beam of polarised X-rays (i.e., with a well-defined direction of $\boldsymbol{E}$, identified by the unit vector $\boldsymbol{\epsilon}$) impinging on a free electron (again, refer to the scheme in fig. 1). The particle with be accelerated by the electric field $\boldsymbol{\epsilon} E_0 e^{-i\omega t}$ of the incoming wave so that

$$\mathbf{a}(t) = \frac{(-e)}{m} \boldsymbol{\epsilon} E_0 e^{-i\omega t} \tag{4}$$

Substituting eq. 4 into eq. 1 we obtain:

$$\mathbf{E}(R,t) = \frac{e^2}{4\pi\epsilon_0 mc^2} E_0 \frac{e^{-i\omega(t-R/c)}}{R} \left[\mathbf{n} \times (\mathbf{n} \times \boldsymbol{\epsilon})\right] = \frac{e^2}{4\pi\epsilon_0 mc^2} E_0 \frac{e^{i(kR-\omega t)}}{R} \left[\mathbf{n} \times (\mathbf{n} \times \boldsymbol{\epsilon})\right] \tag{5}$$

where $k = \dfrac{\omega}{c}$ is the wavenumber. The quantity $r_0 = \dfrac{e^2}{4\pi\epsilon_0 mc^2} = 2.82 \times 10^{-15}$ m is known as the **classical electron radius**. By applying eq. 2 once again we find that the expression in square bracket on the right side of eq. refeq: induced acceleration is

$$\left[\mathbf{n} \times (\mathbf{n} \times \boldsymbol{\epsilon})\right] = -\left[\boldsymbol{\epsilon} - (\boldsymbol{\epsilon} \cdot \mathbf{n})\, \mathbf{n}\right] \tag{6}$$

i.e., it is *minus* the component of $\boldsymbol{\epsilon}$ *perpendicular* to $\mathbf{n}$.

The scattered polarisation ϵ' is the *projection of the incident polarisation perpendicular to the line of sight.*

It is useful at this point to introduce two orthogonal reference components of $\boldsymbol{\epsilon}$ and of the scattered polarisation $\boldsymbol{\epsilon}'$, according to the scheme shown in fig. 2: $\boldsymbol{\epsilon}_\pi$ and $\boldsymbol{\epsilon}'_\pi$ are in the "scattering plane", defined by the incident and outgoing directions, whereas $\boldsymbol{\epsilon}_\sigma = \boldsymbol{\epsilon}'_\sigma$ are *perpendicular* to the scattering plane and are equal. We can decompose the incident polarisation as

$$\boldsymbol{\epsilon} = \cos\xi\, \boldsymbol{\epsilon}_\sigma + \sin\xi\, \boldsymbol{\epsilon}_\pi \tag{7}$$

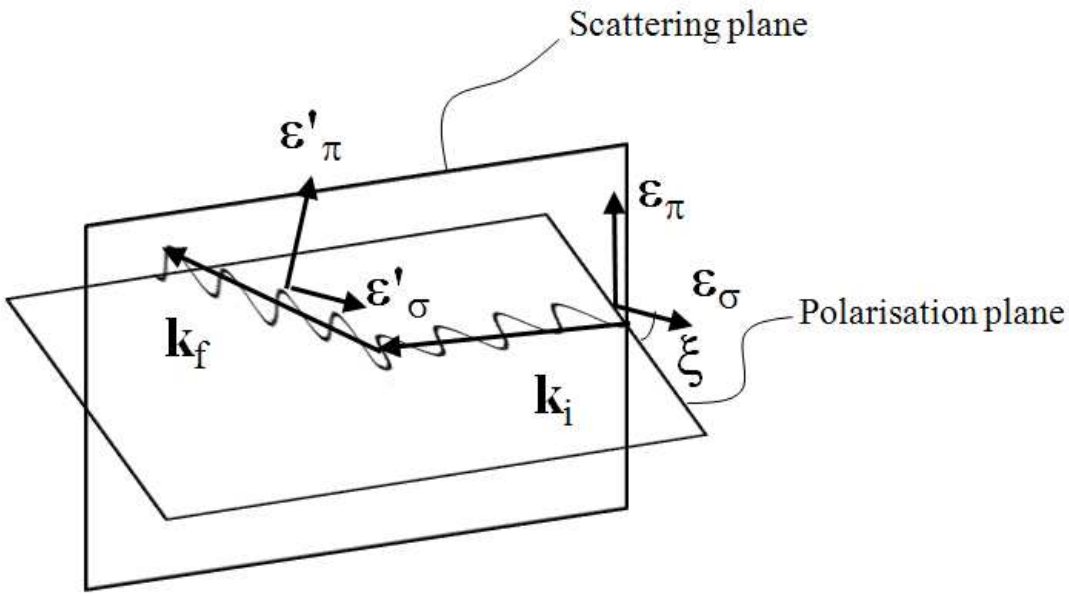

Figure 2: Diagram illustrating the convenstional σ and π reference directions for the incident and scattered polarisation. Note that $\boldsymbol{\epsilon}_\sigma \cot \boldsymbol{\epsilon}'_\sigma = 1$ *always*. Conversely, $\boldsymbol{\epsilon}_\pi \cot \boldsymbol{\epsilon}'_\pi < 1$ **depends on the scattering angle** γ, and **vanishes** for $\gamma = 0$.

so that the incident wave has σ-polarisation for $\xi = 0$ and π-polarisation for $\xi = \frac{\pi}{2}$. The incident polarisation makes an angle ξ with the vector $\boldsymbol{\epsilon}_\sigma$. With a little geometry we conclude

$$\mathbf{E}(R,t) = -r_0\, E_0 \frac{e^{i(kR-\omega t)}}{R} \left[\cos\xi\, \boldsymbol{\epsilon}'_\sigma + \sin\xi\, \cos\gamma\, \boldsymbol{\epsilon}'_\pi\right] \tag{8}$$

where γ is the angle between the incident and scattered wavevector (this angle is also known, by longstanding diffraction convention, as 2θ). Based on eq. 8, we can make the following observations:

- A plane wave impinging on a quasi-free charge produces a scattered *spherical* wave $\frac{e^{i(kR-\omega t)}}{R}$, with an amplitude that in general depends on the scattering angle γ.
- If the incident wave is σ-polarised, the scattered wave is σ'-polarised, and has amplitude $\frac{r_0}{R}\, E_0$.
- If the incident wave is π-polarised, the scattered wave is π'-polarised, and has amplitude $\frac{r_0}{R}\, E_0\, \cos\gamma$.
- The intensity of the scattered wave is zero for scattering of π polarisation at $90°$.
- The scattered wave has a phase shift of π upon scattering (*minus* sign).

The instantaneous energy flux of the scattered wave is given by the Poynting vector:

$$\mathbf{S} = \mathbf{E} \times \mathbf{H} = \epsilon_0 c |\mathbf{E}|^2 \, \mathbf{n} \tag{9}$$

The *average* power radiated per unit solid angle in *both* polarisations is therefore

$$\frac{dP}{d\Omega} = R^2 \, \langle |\mathbf{S}| \rangle = \frac{\epsilon_0 c}{2} R^2 \, |\mathbf{E}|^2 = \frac{\epsilon_0 c \, r_0^2}{2} \, E_0^2 \, \left[\cos^2 \xi \, + \sin^2 \xi \, \cos^2 \gamma \right] \tag{10}$$

It can also be shown that the power radiated for an arbitrary final polarisation $\boldsymbol{\epsilon}'$ is

$$\left(\frac{dP}{d\Omega} \right)_{\boldsymbol{\epsilon}'} = \frac{\epsilon_0 c \, r_0^2}{2} \, E_0 \, \left[\boldsymbol{\epsilon} \cdot \boldsymbol{\epsilon}' \right]^2 \tag{11}$$

As appropriate for a scattering process, it is convenient at this point to introduce the *cross section*, defined as the average power radiated per unit solid angle divided by the average incident power per unit area (power flux, Φ), which is

$$\Phi = \frac{\epsilon_0 c}{2} E_0^2 \tag{12}$$

The cross section into both final polarisation channels (i.e., if the scattered beam is measured *without* an analyser) is therefore

$$\frac{d\sigma}{d\Omega} = r_0^2 \, \left[\cos^2 \xi \, + \sin^2 \xi \, \cos^2 \gamma \right] \tag{13}$$

whereas for an arbitrary final polarisation $\boldsymbol{\epsilon}'$ is

$$\boxed{\left(\frac{d\sigma}{d\Omega} \right)_{\boldsymbol{\epsilon}'} = r_0^2 \left[\boldsymbol{\epsilon} \cdot \boldsymbol{\epsilon}' \right]^2} \tag{14}$$

For an *unpolarised* X-ray beam, for which all the angles ξ are equally represented, the cross section becomes

$$\boxed{\frac{d\sigma}{d\Omega} = r_0^2 \left[\frac{1 + \cos^2 \gamma}{2} \right]} \tag{15}$$

NOTE: our discussion on the incident and final polarisations is relevant because different X-ray sources have different characteristics. The beam from a typical lab X-ray machine is unpolarised, and so eq. 15 applies. Synchrotron radiation is naturally polarised in the plane of the electron orbit,so that $\xi = 0$ in eq. 13. Unlike the case of lab machines, synchrotron diffractometers have a *vertical* scattering plane, so that the $90°$-cross section does not vanish. Synchrotron beamlines specifically designed for resonant or magnetic scattering often have the ability to change the incident polarisation to the π channel or even to produce circularly-polarised X-rays. in addition, it is possible to *analyse* the scattered polarisation as well.

2.2 Thomson scattering from many quasi-free electrons

The Thomson formula can be easily extended to the case of multiple scattering centres, provided that the amplitude of the motion of each electron is small with respect to the wavelength. What we aim to achieve is to find an expression for the X-ray scattering amplitude and cross section of **a multi-electron atom**. In this case, the radiation emitted by each electron at position $\mathbf{x}_i$ will be characterised by an approximately *time-independent* phase factor $e^{i\mathbf{k}\cdot\mathbf{x}_i}$, accounting for the fact that the charge is not at the origin, $\mathbf{k}$ being the wavevector of the incident radiation. Also, the radius R in eq. 8 needs to be replaced with individual radii R_i. Here, we can employ the very useful trick of approximating

$$R_i \approx R - \mathbf{n}\cdot\mathbf{x}_i \tag{16}$$

This is equivalent to considering diffraction in the "far field" limit (*Fraunhofer diffraction*). Eq. 16 can be obtained by writing the vector relation;

$$R = |\boldsymbol{R}| = |\boldsymbol{R}_i - \boldsymbol{x}_i| = |R_i\boldsymbol{n} - \boldsymbol{x}_i| \tag{17}$$

and expanding it to the quadratic term in x_i/R; is certainly valid in the case we are interested in, where the distances between scattering centres are comparable to atomic sizes whereas R (the experimental scattering path) is macroscopic. By summing the amplitudes of individual scattering centres we obtain

$$\begin{aligned}\mathbf{E}(R,t) &= -r_0 E_0 \tfrac{e^{i(kR-\omega t)}}{R}\left[\boldsymbol{\epsilon}\cdot\boldsymbol{\epsilon}'\right]\textstyle\sum_i e^{i(\mathbf{k}_i-\mathbf{k}_f)\cdot\mathbf{x}_i} \\ &= -r_0 E_0 \tfrac{e^{i(kR-\omega t)}}{R}\left[\boldsymbol{\epsilon}\cdot\boldsymbol{\epsilon}'\right]\textstyle\sum_i e^{-i\mathbf{q}\cdot\mathbf{x}_i}\end{aligned} \tag{18}$$

where $\mathbf{k}_i$ and $\mathbf{k}_f$ are the incident and scattered wavevectors and $\mathbf{q} = \mathbf{k}_f - \mathbf{k}_i$.[1] Note the important formula, valid for elastic scattering (we recall that $\gamma = 2\theta$):

$$q = |\mathbf{q}| = \frac{4\pi \sin\theta}{\lambda} \tag{19}$$

Eq. 19 is illustrated graphically in fig. 3

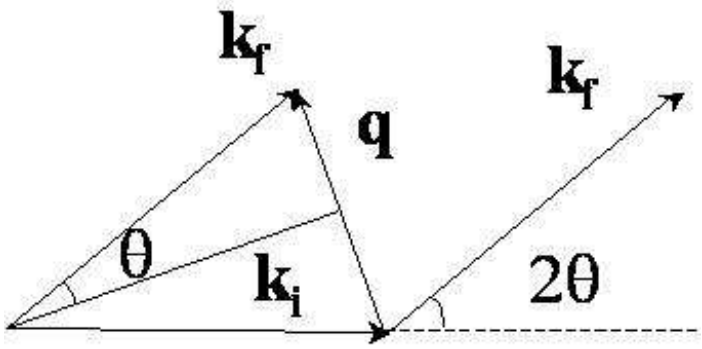

Figure 3: Scattering triangle for elastic scattering.

We can extend this result to a *continuous* distribution of charges by replacing the sum over discrete charges with an integral over the electron density $\rho(\mathbf{r})$

$$\mathbf{E}(R,t) = -r_0 E_0 \frac{e^{i(kR-\omega t)}}{R} \left[\boldsymbol{\epsilon} \cdot \boldsymbol{\epsilon}'\right] \int \rho(\mathbf{x}) e^{-i\mathbf{q}\cdot\mathbf{x}} d\mathbf{x} \tag{20}$$

The integral

$$\boxed{f(\mathbf{q}) = \int \rho(\mathbf{x}) e^{-i\mathbf{q}\cdot\mathbf{x}} d\mathbf{x}} \tag{21}$$

is known as the **atomic scattering factor or form factor**.

[1] Throughout this part of the course, we will employ the convention that $\boldsymbol{q}$ is *the change of wavevector of the particle or photon*, so $\boldsymbol{q} = \boldsymbol{k}_f - \boldsymbol{k}_i$. the convention $\boldsymbol{q} = \boldsymbol{k}_i - \boldsymbol{k}_f$ identifies $\boldsymbol{q}$ with the wavevector *transferred to the crystal*, and is widely employed particularly in the context of inelastic scattering

We have arrived here at an important result: **the scattering amplitude for many quasi-free electrons is proportional to the Fourier transform of the charge density**. Note that the integral for $\mathbf{q} = 0$ is the **total charge**, which for an atom is the atomic number Z (fig. 4).

A key fact to remember: the *more spread out* the charge is around the atom, the *faster* $f(\mathbf{q})$ will decay at high q.

High q $\equiv$ high scattering angles, short wavelengths.

Eq. 20 can be further simplified in the case of a spherically symmetric charge distribution (the development is straightforward by converting to polar coordinates with the z axis along **q**):

$$f(q) = 4\pi \int_0^\infty dr\, r^2\, \rho(r) \frac{\sin qr}{qr} \tag{22}$$

The cross sections are obtained in the same way as for a single charge — for instance, the unpolarised cross section for an atom is:

$$\left(\frac{d\sigma}{d\Omega}\right)_{atom} = r_0^2 \left|f(\mathbf{q})\right|^2 \left[\frac{1+\cos^2\gamma}{2}\right] \tag{23}$$

which, in forward scattering, becomes:

$$\left(\frac{d\sigma}{d\Omega}\right)_{atom} = r_0^2\, Z^2 \left[\frac{1+\cos^2\gamma}{2}\right] \tag{24}$$

One can find tabulated values for neutral and ionised atoms in the International Tables for Crystallography, volume C [1], p 555 and p 566, respectively.

2.3 X-ray absorption: the photo-electric effect and X-ray fluorescence

When the beam of X-rays impinges at normal incidence on a slab of material of thickness L, it suffers both scattering and absorption, and is therefore ***attenuated*** according to the familiar equation:

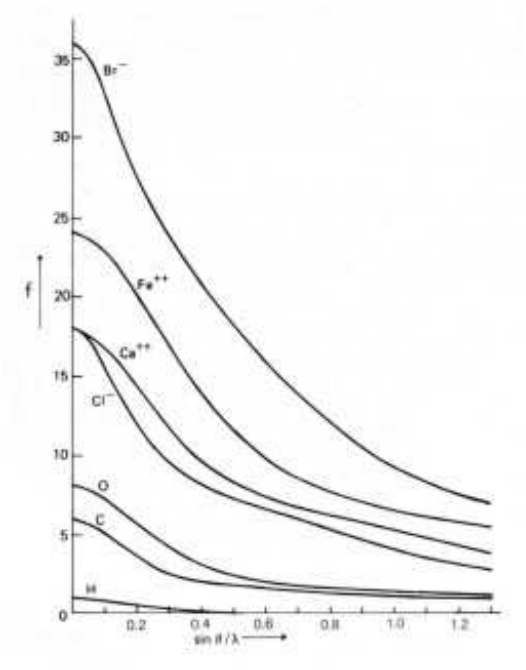

Figure 4: Atomic scattering factors (form factors) for selected neutral atoms and ions. Note that $\sin\theta/\lambda = q/4\pi$.

$$I = I_0 e^{-\mu L} \tag{25}$$

where μ is the **linear attenuation coefficient**, which is related to the **total cross section** σ_{tot} (scattering plus absorption) by the equation:

$$\mu = \sigma_{tot}\, N_a \tag{26}$$

where N_a is the number of scattering/absorption centres (here atoms) per unit volume. Fig. 5 shows a comparison of the cross sections of different processes leading to X-ray attenuation in materials.

At X-ray energies used in typical experiments (5–50 KeV), *the photo-electric absorption cross section is by far the largest contributor to X-ray attenuation*.

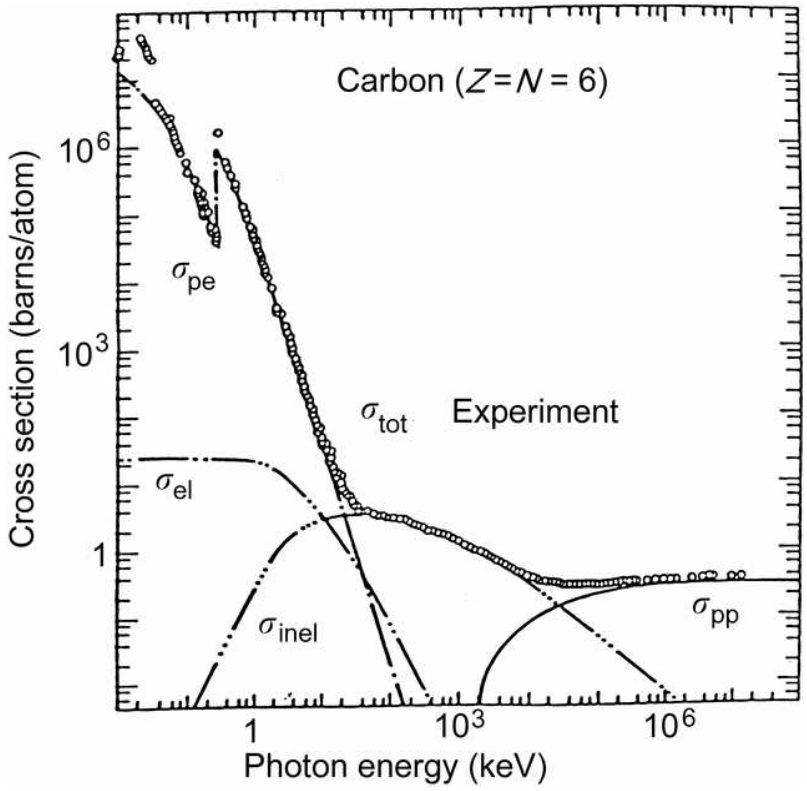

Figure 5: Contributions to the X-ray scattering and absorption cross section for the element carbon (C), from the International Tables for Crystallography, vol. C [1], p 213. In this figure, σ_{el} is the Thomson cross section, σ_{inel} is the Compton inelastic cross section and σ_{pp} is the pair-production cross section, whereby a high-energy photon produces an electron-positron pair. Note the K absorption edge in the photo-electric cross section at 284.2 eV

Key facts about the photoelectric absorption of X-rays

- In the photo-electric absorption process, a photon is completely absorbed and the energy is transferred to a **core electron** (i.e., an electron in the inner atomic shell), which is excited into unoccupied bound states above the Fermi energy or in the continuum.
- The key parameter controlling this effect is, naturally, the **electron binding energy**, which is typical of each shell and atom or ion. **No photoelectric absorption can take place if the photon energy is *lower* than the binding energy of the electron**. This is in complete analogy with the more familiar photo-electric effect in semiconductors. As the photon energy is increased through a binding energy "threshold", **additional absorption can take place**, so absorption increases abruptly. This is known as an **absorption edge** (see fig. 6).
- Binding energy are classified based on the **quantum numbers of the core electron**. **A letter indicates the principal quantum number of the core electron**, so "K" for n=1, "L" for n=2, "M" for n=3 "N" for n=4 and so on. This is followed by a **roman subscript** indicating energy sub-levels. Therefore, the K edge indicates a transition from the $1s$ core state. L_I, L_{II} and L_{III} indicate transitions from the $2s$, $2p_{1/2}$ and $2p_{3/2}$, respectively ($2p_{1/2}$ and $2p_{3/2}$ having distinct values of the *total* angular momentum J).

- An X-ray photo-electric absorption event is followed by a chain of **X-ray emission (or fluorescence) events** whereby the excited atom gradually relaxes to the ground state. The processes of absorption and subsequent re-emission are shown schematically in fig. 7. Strong emission lines are those that follow the **dipole selection rules**, i.e., $\Delta l = \pm 1$ and $\Delta j = 0, \pm 1$. For example, for transition metals, there are 3 strong emission lines: $K_{\alpha 1}$ and $K_{\alpha 2}$ for transitions from $2p_{1/2}$ and $2p_{3/2}$ to $1s$ and K_β for transitions from $3p$ to $1s$. X-ray emission is extensively employed to produce monochromatic X-ray radiation (see below).

- **Far from absorption edges, photo-electric absorption decreases as a function of photon energy**, following the very approximate law:

$$\sigma_{ph} \propto \frac{Z^n}{(\hbar\omega)^3} \tag{27}$$

  where Z is the atomic number and the exponent is a number between 4 and 5.

- A list of characteristic absorption and emission X-ray energies can be found in the International Tables for Crystallography, vol. C [1], starting from p 206.

2.4 X-ray scattering beyond the free-electron approximation

Up to now, we have left the issue of "free" electrons somewhat ambiguous. Truly "free' electrons (e.g., conduction electrons in a metal) hardly contribute to the scattering of X-rays, because their probability distribution extends a long way throughout the crystal, and, from eq. 21, the form factor decays very rapidly away from forward scattering (fig. 4). Conversely, the largest contribution to X-ray scattering from atoms is given by "core" electrons, which are close to the nucleus and have slowly decaying from factors — but these electrons are certainly not free! Indeed, there are large departures from the Thomson scattering formula near *atomic resonances*, where the energy of the photon is just sufficient to eject an electron from a core state into the continuum. As we shall briefly see later, away from resonances, the Thomson formula can be corrected to a very good approximation by replacing the form factor by the *complex* quantity

$$\boxed{f(\mathbf{q}) = f_{Thom}(\mathbf{q}) + f'(\hbar\omega) + if''(\hbar\omega)} \tag{28}$$

where the so-called *anomalous terms*, f' and f'', away from atomic resonances do not depend on q and are weak functions of the photon energy.

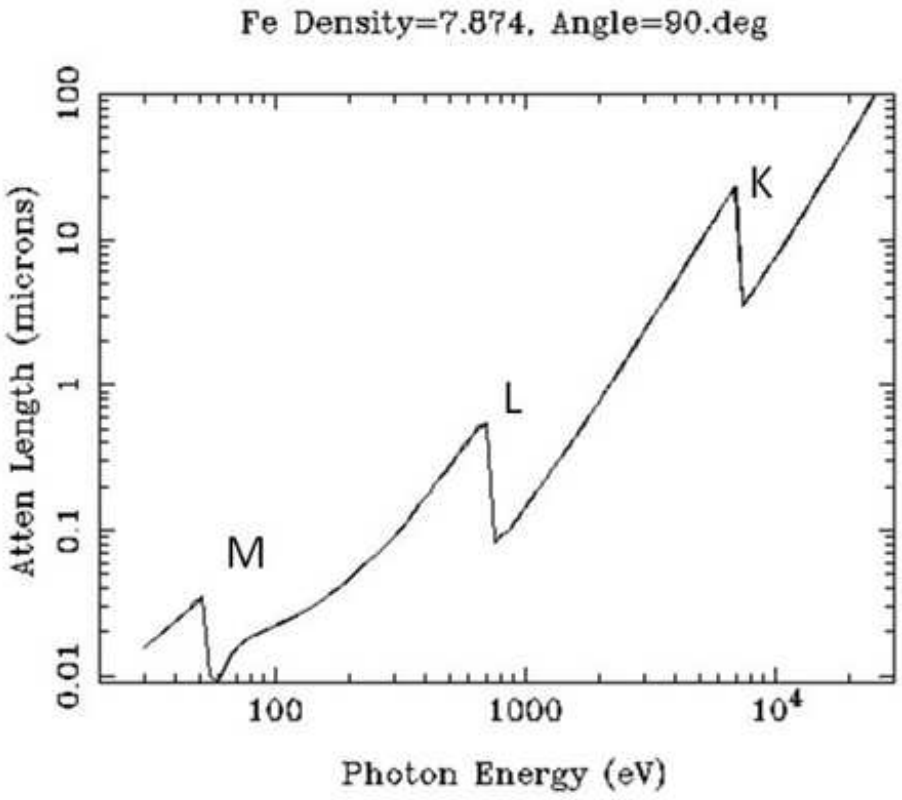

Figure 6: Attenuation length $(1/\mu)$ in microns for elemental iron (Fe), in the energy interval between 30 eV and 25 KeV. The figure was generated using the attenuation calculator in http://henke.lbl.gov/optical_constants/atten2.html. Note the three absorption edges: K at 7.112 KeV, L (actually three edges at 845 eV, 720 eV and 707 eV) and M (edges at 90 eV and 50 eV).

A simple justification of eq. 28 is given in Appendix I.

It can be shown, as a consequence of the so-called optical theorem, that *the imaginary part of the scattering factor is proportional to the linear absorption coefficient due to the photoelectric effect* (see below).

$$f''(\hbar\omega) = \frac{\omega}{4\pi r_0 c N_a}\mu \tag{29}$$

where N_a is the number of atoms per unit volume, and the other symbols have the usual meaning. The quantity μ is the *linear absorption coefficient*, defined in eq. 25.

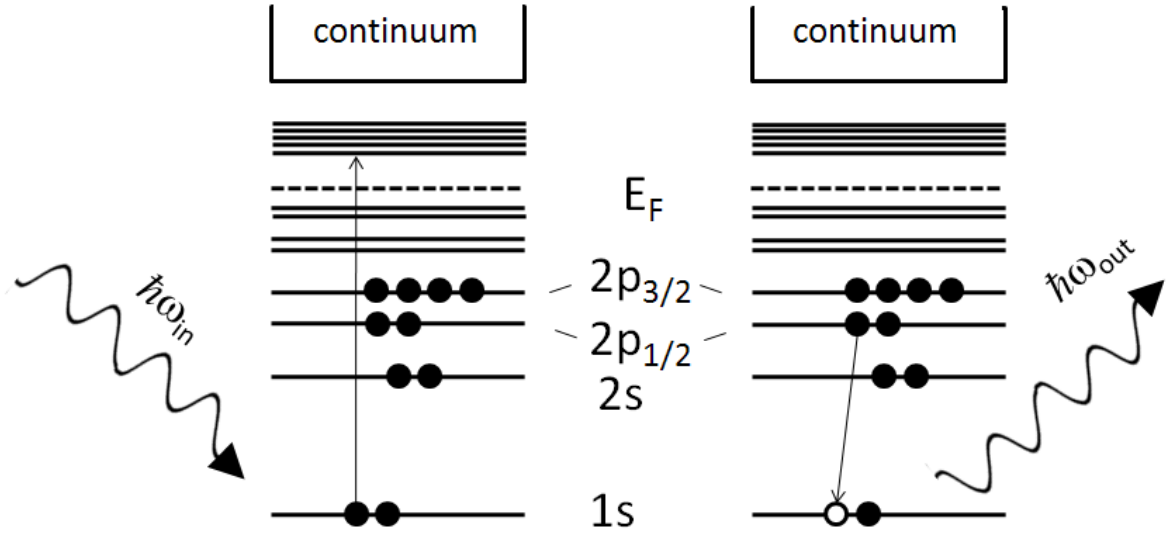

Figure 7: Schematic representation of the absorption and subsequent emission for a K edge event. **Left**: a photon with energy above the K edge is absorbed and an $1s$ electron is ejected above the Fermi energy or into the continuum. **Right**: an electron in the $2p_{1/2}$ shell makes a transition to fill the $1s$ core hole, resulting in the emission of a photon with the characteristic energy $K_{\alpha 2}$.

3 Thermal neutron and electron scattering from atoms and spins

3.1 Introduction

Up to this point, we have carefully examined the case of X-ray scattering from electrons and atoms. One important result we have obtained (for example, see eq. 8) is that

The scattering process generates a *spherical wave*, the *squared* amplitude of which is proportional to the cross section.
This result is completely general, and, within the framework of the approximations we have used, is valid for electron-electron scattering as well as for thermal neutron scattering from nuclei and from magnetic moments. As in the case of photons, we will therefore have to calculate the *scattering amplitudes* from individual scatterers.
If multiple scattering centres are present, we will **sum up the amplitude from the individual centres with the appropriate phase**.

Naturally, the wave-like nature of particle beams (neutrons and electrons) is *essential* in deriving these results, so, unlike the case of photons, we will have to work within the framework of quantum mechanics.

A rather extensive derivation of the scattering amplitudes and cross sections for electron and neutron scattering is contained in Appendix II. In the following paragraphs, we will quote the most important results and formulas and provide a *qualitative* description of the relevant physics.

3.2 Elastic scattering of electrons from atomic charges

- Electrons are elastically scattered by the Coulomb potential of the nuclei (*attractive*) and of other electrons (*repulsive*).
- Electron scattering is **much stronger than Thomson scattering**. Therefore, The single-event scattering approximation we have employed so far is of limited use, and a full "dynamical" treatment is essential to obtain quantitative information about charge densities.
- Within the range of validity of the kinematic approximation (e.g., very thin samples of light atoms), the **electron scattering amplitude $f^B(q)$ can be calculated as a function of the X-ray form factor f_X**

$$f^B(q) = \left(\frac{e^2}{\epsilon_0}\frac{m}{2\pi q^2\hbar^2}\right)(Z - f_X(q)) \tag{30}$$

- One can get a good idea of the huge difference between electron and X-ray cross sections by comparing their scattering amplitude for $q = 0$ (both are expressed in metres)

$$\begin{aligned} r_0 f_X(0) &= r_0\, Z = 2.82 \times 10^{-15}\, Z \quad \mathbf{X-rays} \\ f^B(0) &= \frac{2}{3}\left(\frac{e^2}{\epsilon_0}\frac{m}{2\pi\hbar^2}\right) Z < r^2 >= 2.23 \times 10^{-10} Z < r^2 > \quad \mathbf{electrons} \end{aligned} \tag{31}$$

  where $< r^2 >$ is the **mean squared atomic radius expressed in Å**, which is typically of the order of $0.2 - 2\mathring{A}^2$

  the electron elastic scattering amplitude is 4-5 order of magnitudes *larger* than the X-ray scattering amplitude

3.3 Properties of thermal neutrons

- Free neutrons are unstable, with half-life τ = 10.6 min. (β-decay)
- Neutrons bound in nuclei are (generally) stable.
- Mass: $1.67492729(28) \times 10^{-27}$ kg

- Electric dipole moment $D < 10^{-25}$ (e cm)
- Spin: s = $\frac{1}{2}$ — neutrons are *fermions*.
- Magnetic dipole moment: $\mu = -1.9130418\ \mu_N$, where $\mu_N = \frac{e\hbar}{2m_p} = 5.05078324(13) \times 10^{-27}$ JT^{-1} is the **nuclear magneton**.

Table 2: Neutron wavelenghts and kinetic energies in different "slow" ranges. The thermal energy per particle at room temperature is 25 meV.

	λ (Å)	E (meV)
Cold	3–30	0.1-10
Thermal	1–3	10–100
Hot	0.4–1	100–500
Epithermal	< 0.4	> 500

3.4 Elastic scattering of thermal neutrons

Neutrons are elastically scattered by the condensed matter through two completely different mechanisms, but, as it turns out, yielding comparable scattering lengths.

1. By **nuclear interaction with the atomic nuclei**.
2. By **dipole interaction with the unpaired spin and orbital magnetic moments of the atoms**. This is only present if the atom or ion has a magnetic moment.

A rather complete description of these interactions is contained in Appendix II. A summary of the key result is provided here below.

Neutron-nuclear interaction

- The neutron-nuclear interaction is **isotope and elements specific**, and **depends on the mutual orientation of the neutron and the nuclear spin**.
- As far as neutron crystallography is concerned, **the key parameter is the scattering amplitude *averaged* over the nuclear spin states**, known as the **coherent scattering amplitude**.
- The neutron nuclear coherent scattering amplitude **is independent on q** — it carries **no form factor**, and is therefore expressed by a single number, known as the **Fermi length**.
- **Fermi lengths can be positive or negative, depending on whether the neutron-nuclear interaction is attractive or repulsive**. For typical nuclei, they are of the order of a few fm (10^{-15} m) (see fig 8), which means that they **are comparable to the classical electron radius**. However, atoms have a single nucleus and many electrons, so X-ray scattering cross sections in the *forward* direction are typically much larger than neutron cross sections (X-ray cross sections decay at high q due to the form factor).
- Fermi lengths do not vary in a systematic way across the periodic table (fig 8), which means that **with respect to X-rays, neutrons are uniquely sensitive to some light elements — notably oxygen**. The different scattering lengths of different isotopes is also widely exploited in the so-called **contrast variation techniques.**

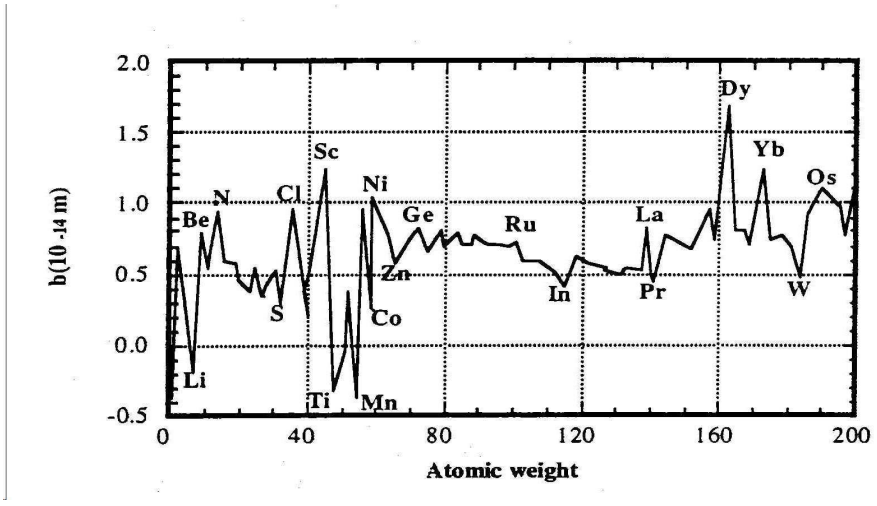

Figure 8: Variation of the Fermi length as a function of atomic weight.

Neutron-magnetic interaction

- When the scatterer carries a magnetic moment, in addition to the normal nuclear interaction, neutron are also scattered by dipole-dipole interaction from the magnetic moment of the atom.
- Magnetic scattering of neutrons is governed by the following **vector** scattering amplitude.

$$\boldsymbol{A}_n = \gamma_N r_0 f_m(\boldsymbol{q}) \mathbf{M}_\perp \tag{32}$$

  where γ_N is the neutron gyromagnetic ratio (-1.9130418), r_0 is the familiar **classical electron radius** and $\mathbf{M}_\perp$ is the **projection of the atomic magnetic moment *perpendicular* to the wavevector transfer $\boldsymbol{q}$**, and is expressed in **Bohr magnetons**.
- The quantity $f_m(\boldsymbol{q})$ is known as the **neutron magnetic form factor**, and is normalised so that $f_m(0) = 1$. It is similar to the X-ray form factor, except for the fact that it only include the more extended **density of unpaired electrons**. Therefore **magnetic neutron scattering decays very rapidly at high** q.
- From eq. 32 one can obtain a **number of cross sections**, accounting for the different orientations of the neutron spin with respect to the atomic magnetic moment (***neutron polarisation***). The most important cross section is the **unpolarised neutron cross section** (averaged over all the possible neutron polarisations), which, for a *single* atom, is:

$$\frac{d\sigma}{d\Omega} = \gamma_N^2 r_0^2 f_m^2(\boldsymbol{q}) |\mathbf{M}_\perp|^2 \tag{33}$$

- Typical magnetic moments for atoms and ions are **a few Bohr magnetons**. Therefore, from eq. 33, one finds that **neutron nuclear and magnetic scattering cross sections are typically comparable in magnitude for magnetic atoms.**

- Although X-rays are also scattered by magnetic moments, in both resonant and non-resonant conditions, **the magnetic scattering cross section for neutrons is several orders of magnitude greater than that of X-rays. This makes neutrons the technique of choice to study magnetic structures**. X-ray magnetic scattering has some unique advantages, and is steadily gaining in popularity thanks to the advent of powerful synchrotron sources.

3.5 Absorption of thermal neutrons

When a thermal neutron collides with a nucleus, it may be scattered or absorbed. Absorption process are those in which there is no neutron in the final state; they can be either **neutron capture** (known as (n, γ)), in which the mass number of the final nucleus is increased by 1 unit, or a **transfer reactions**, in which the mass number of the final nucleus is decreased and an α particle ((n, α)) or a proton ((n, p)) is emitted. Here are some examples:

$$\begin{array}{ll} (n,\gamma) & {}^{197}Au + n \rightarrow {}^{198}Au + \gamma \quad \textbf{Neutron capture by gold} \\ (n,p) & {}^{3}He + n \rightarrow {}^{3}H + p \quad \textbf{Triton/proton production} \\ (n,\alpha) & {}^{10}B + n \rightarrow {}^{7}Li + \alpha \quad \textbf{Alpha production} \\ (n,\alpha) & {}^{6}Li + n \rightarrow {}^{3}H + \alpha \quad \textbf{Triton/alpha production} \end{array} \tag{34}$$

Reactions such as those in eq. 34 are extensively used in the process of neutron detection and to fabricate neutron shields. In general, we can say that

Neutron absorption

- Thermal neutrons are **weakly absorbed** by most materials, with typical absorption lengths of the order of a cm.
- **Neutrons with longer wavelengths are more strongly absorbed**. For most materials, **absorption cross sections are proportional to the neutron wavelength**, so the absorption lengths are inversely proportional to the wavelength.

4 X-ray production and detection

4.1 Introduction

In this section, we will briefly describe the most important methods of X-ray production, both in the laboratory and at large-scale facilities. We will also spend a few words on X-ray detectors, although this description will be necessarily incomplete given the time restrictions in this course and the magnitude of the subject.

4.2 X-ray tubes

The most common and ubiquitous source of X-rays is the **high-vacuum tube**, illustrated schematically in fig. 9. Conceptually, the X-ray tube has not changed greatly from the one built by W. Roentgen (Nobel prize 1901). It consists of an **electron gun** — usually a thermoionic cathode —, which produces a well-defined, mono-energetic beam of electrons. It is usually desirable to concentrate the electron beam in a small, intense spot, but other configurations (e.g., "line focus") are possible for particular applications. Typical laboratory devices are completely **sealed tubes**, and run at 40–60 KV (up to over 100 KV for heavy-metal anodes) and 30-40 mA, for a total power up to 3-6 KW. Higher powers require the **rotating anode** design to avoid excessive power loads, but this requires active vacuum pumping and a rotary seal, which is less reliable. Recently, the **microfocus sealed tube** has become increasingly popular, achieving a small, extremely intense spot with very low overall power loads ($\sim$ 40 W).

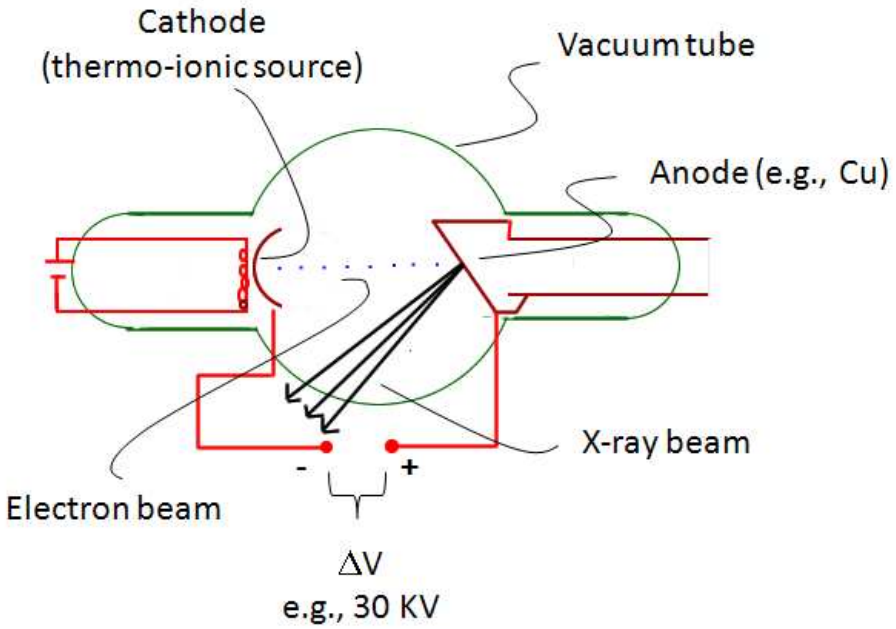

Figure 9: Schematic representation of an X-ray vacuum tube.

4.2.1 X-ray tube spectrum

A typical spectrum from an X-ray tube is shown in fig. 10 and consists of 2 components:

- The **continuous spectrum**, or **"bremsstrahlung"** (="breaking radiation"). This part of the spectrum is produced by the rapid deceleration of the electrons in the anode, due to a variety of processes.

- The **characteristic lines**, or **emission lines**. These are due to atoms in which one of the **core electrons** has been ejected, due to interaction with the incoming electron beam. **The energy of the characteristic lines is the same as that of X-ray emission lines, such as** $K_{\alpha 1}$**,** $K_{\alpha 2}$**,** K_{β} **etc.** (see section 2.3.)

- For monochromatic experiments, one generally employs the very intense **characteristic lines**. The bremsstrahlung and some/all the other lines can be removed either by using a monochromator (or analyser, see next lecture) or by a **photon energy discriminator** in the detector.

- The maximum photon energy is equal to the electron beam energy.

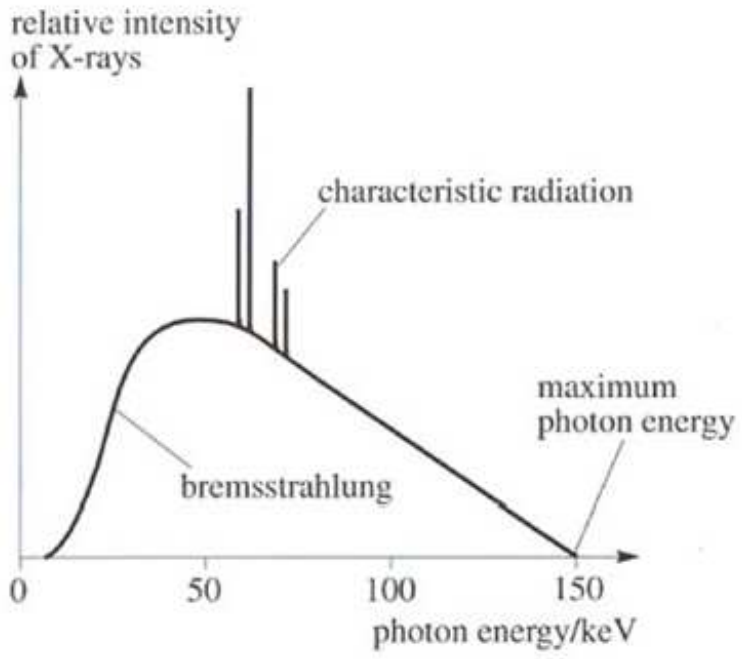

Figure 10: Typical spectrum of an X-ray tube.

4.3 Synchrotron sources

As we have seen at the beginning of this lecture, an accelerated charge emits electromagnetic radiation. The characteristic radiation of a **charged particle in circular motion** is known as ***synchrotron radiation***. *Parasitic* synchrotron radiation was produced in cyclotrons (since the work of Ernest Lawrence (1929)) and early particle accelerators , but it was not until the late seventies that the first synchrotrons *dedicated to producing synchrotron radiation* were conceived. The first synchrotron of this kind with the Synchrotron Radiation Source in Daresbury, in Cheshire. **All modern synchrotrons accelerate either electrons or positrons.** A concise description is contained in the international Tables for Crystallography vol. C [1], p 195. A complete derivation of the relativistic case is given in [3], p 654f.

Key facts about synchrotron radiation

- The **power** radiated by a charge in circular motion is proportional to the *fourth power of the electron energy*, according to the formula:

$$P(\mathrm{KW}) = 8.85 \times 10^{-2} \frac{[E(\mathrm{GeV})]^4}{R(\mathrm{m})} I(\mathrm{mA}) \tag{35}$$

  where I is the circulating current (in mA), R is the radius of the machine in metres and E is the electron energy in GeV. For example, for the Daresbury synchrotron, $R = 5.5\mathrm{m}$, $E = 2\mathrm{GeV}$, $I = 200\mathrm{mA}$ and $P = 51.5\mathrm{KW}$.

- In a synchrotron, the energy lost in the form of synchrotron radiation has to be restored to the circulating electrons by a series of **microwave cavities**. The electrons themselves are maintained in orbit by a series of **bending magnets**, which alternate with the cavities and with magnetic focusing lenses to define and control the electron beam.

- In the non-relativistic limit, radiation would be emitted over the whole solid angle. However, at these energies (several GeV), the electrons are in the **extreme relativistic limit**, and **emit radiation only in a narrow vertical fan**. The opening angle is $\psi = mc^2/E \approx 25\mathrm{mrad}$ at 2 GeV (see fig 11).

- Synchrotron radiation is essentially **100% polarised in the plane of the orbit**.

- Synchrotron radiation has a **continuous spectrum**, ranging from the infra-red to the hard X-rays and soft γ-rays. An important parameter characterising this spectrum is the **characteristic wavelength**, given by

$$\lambda_c = \frac{4\pi}{3} R(E/mc^2)^3 \tag{36}$$

  The X-ray flux decays very rapidly for wavelengths shorter than the characteristic wavelength (see fig. 12.

- In the early synchrotrons, **synchrotron radiation was emitted primarily at the bending magnets**, and this is where the **beamlines** were located. In modern synchrotrons the most intense radiation is produced by **insertion devices** (known as "wigglers" and "undulators"), where the electrons undergo oscillatory motion.

4.4 X-ray detectors

Here, we have the space only for a fleeting reference to the main X-ray detection technologies — for a complete survey, see the International Tables of Crystallography vol C [1], p 618.

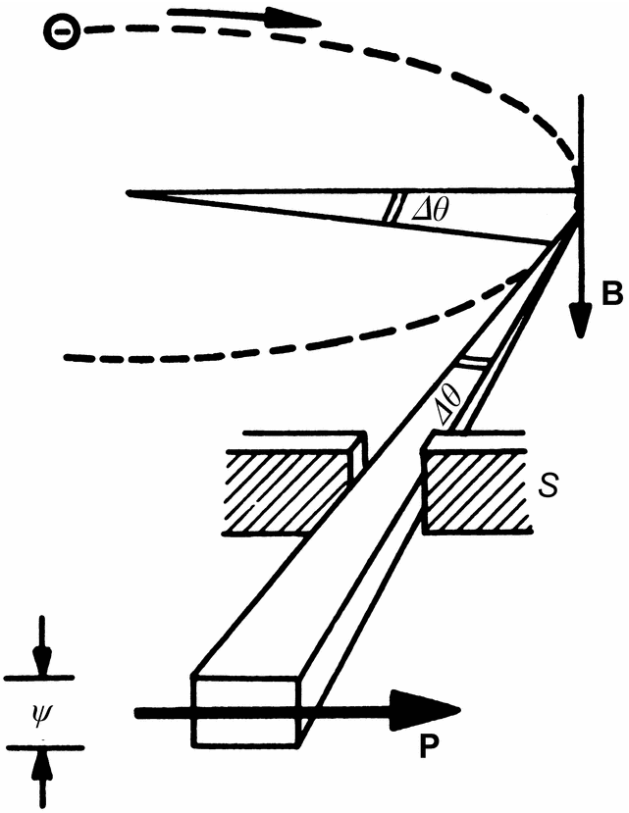

Figure 11: Radiation emitted by a synchrotron in the relativistic limit. The angle ψ is given by $\psi = mc^2/E$. The direction of polarisation is also shown. $\boldsymbol{B}$ is the magnetic field *perpendicular* to the electron orbit, as generated by the bending magnet. The horizontal divergence is limited by means of slits.

Photographic film was the earlies type of X-ray detector, and was still the commonest one until the seventies. Photographic film is still employed in a variety of applications, particularly for Laue diffraction. The **blackening** of the film (expressed in units of density) follows a logarithmic law:

$$D = \log_{10}(I_{incident}/I_{transmitted}) \tag{37}$$

Scintillation counters have two elements: a **fluorescent crystal** and a **photomultiplier tube, or PMT**. The incoming X-ray photon generates a cascade of **visible photons**, which are detected by the PMT. Importantly, **the amplitude of the signal is *proportional* to the energy of the X-ray photon**, so electronic discrimination schemes can be implement to reject certain photon energies (e.g., the bremsstrahlung and/or or the fluorescence generated by the sample).

Proportional gas tubes or ionisation chambers are gas-filled metallic tubes with a central wire anode, maintained at a high voltage with respect to the tube wall. For appropriate parameters of the gas pressure, the amount of charge collected after an ionisation event is

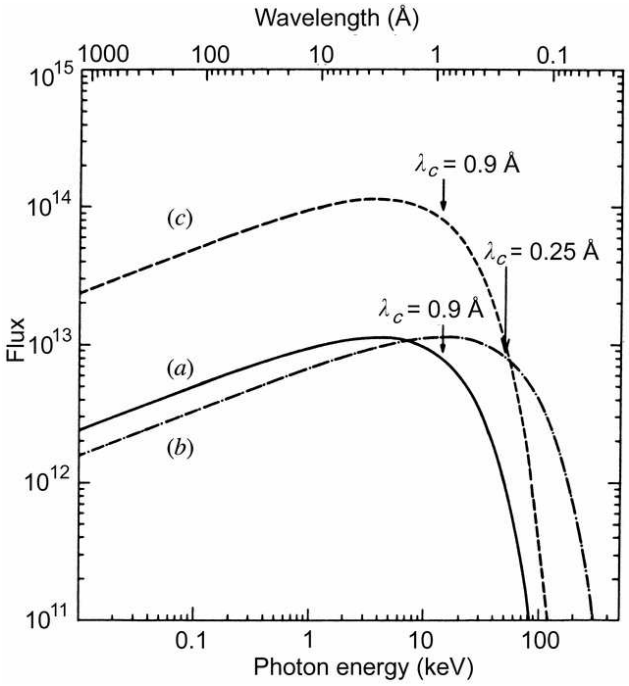

Figure 12: Photon energy spectra for (a) a bending magnet (b) two types of "wigglers" (insertion devices). Note how the flux decays rapidly above the characteristic energy corresponding to λ_c.

proportional to the X-ray photon energy.

Multi-channel semiconductor detectors They are typically high-purity Si or Ge detectors, in which the energy to create an electron/hole pair is 3.9 eV and 3.0 eV, respectively. The number or electron/hole pair produced is proportional to the X-ray photon energy. The charge "drift" in an applied electric field, and appropriate circuitry is implemented to analyse the pulse heights and "store" the counts in a series of **energy channels** ("bins"). This type of detector is popular for **white-beam, energy-dispersive diffraction**.

Position-sensitive detectors (PSDs) produce patterns in either 1 or 2 dimensions. In **image plates**, the X-ray photon energy is stored on a 2-dimensional plate within phosphors, and can be released by stimulation with visible light (photo-stimulated luminescence). The plates are usually "read" using a laser scanner. This method has extremely good spatial resolution and dynamic range, but requires a separate "read" step. **Charge-coupled devices** (CCD's), coupled to a fluorescent screed, are becoming increasingly popular for lab diffractometers. **Solid state PSDs**, which are just coming to the market, have the added advantage of **counting** each X-ray photon rather than simply **integrating** the charge, as is the case for CCDs.

5 Neutron production and detection

5.1 Introduction

The idea that atomic nuclei could contain neutral particles has been formulated essentially since the time of Rutherford, based on the observation that the nuclear masses over most of the periodic table were a bit more than twice the atomic number Z. It was speculated, at some point, that the additional mass could be provided by additional protons and electrons, but it was soon realised that the required confinement energy for electrons was much too large to be compatible with electrostatic interactions.

In 1930, Bothe and Becker made a key experimental observation: bombarding a beryllium target with α particles (from a ^{210}Po source — polonium was discovered by Pierre and Marie Curie in 1898) produced highly-penetrating, *neutral* radiation. The initial speculation was that this was γ radiation, but Curie and Joliot showed that 5.3 MeV protons resulted when bombarding a block of paraffin with this radiation — an observation that is inconsistent with reasonable photon energies. James Chadwick is usually credited with the discovery of the neutron. By bombarding targets such as nitrogen, oxygen and other gasses, he disproved conclusively the photon theory, and was able to calculate the mass of the neutron, obtaining a result that is remarkably close to the modern value (939.57 MeV).

Nowadays, a variety of neutron sources are available. Small, portable neutron sources based on radioactive isotopes or small accelerators are employed commercially for a variety of applications. Neutron sources of relevance for the study of condensed matter are stationary, large-scale facilities employing hundreds of staff and attracting experiments from thousands of scientists every year.

5.2 Radioactive sources of neutrons

The sources originally employed by Bothe and Becker and Chadwick exploited a fusion reaction between α particles (emitted by polonium or radium and light nuclei such as Li, Be or B). For instance

$$^4He + ^9Be \rightarrow ^12C + n + 5.7\,\mathrm{MeV} \tag{38}$$

Modern sealed sources, which are commercially available, usually employ ^{241}Am, ^{238}Pu or ^{239}Pu as sources of α particles.

Another type of isotope-based source contains elements that undergo spontaneous fission, such

as ^{252}Cf.

These types of sources can produce 10^7-10^9 neutrons per second, and are mainly used to calibrate neutron detectors.

5.3 Portable accelerators for neutron production

These sources work by accelerating deuterium (D) ions onto a deuterium or tritium (T) target, exploiting the **fusion** reactions:

$$\begin{aligned} D + D &\rightarrow {}^3He + n + 3.3\,\mathrm{MeV} \\ D + T &\rightarrow {}^4He + n + 17.6\,\mathrm{MeV} \end{aligned} \tag{39}$$

These sources are also commercially available, and can generate in excess of 3×10^9 neutrons per second. The main advantage of the sealed sources is that *they can be turned off*, so are much more practical to use outside nuclear installations, and are employed for **non-destructive materials testing** and for **security applications (radiography)**.

5.4 Reactor sources

Nuclear reactors exploit the **fission** reaction

$$n + {}^{235}U \rightarrow [\text{two fission fragments}] + 2.5n + 200\,\mathrm{MeV} \tag{40}$$

which produces, on 2.5 (on average) neutrons per fission event (fig 13). Of these, 1 is requires to maintain the chain reaction, 0.5 are absorbed and 1 escapes the core and is available for use. The **nuclear cross section** for the reaction in eq. 40 is about ~ 1 **barn for the fast neutrons** emerging from the fission event, but is **1000 barns for slow thermal neutrons** (thermal energies in the tens of meV range). Therefore, in most reactor designs, neutrons are slowed down (**thermalised**) by means of a **moderator** — typically **graphite** (as in the Chicago pile CP-1, December 2, 1942), **water** or **heavy water**.

The reactors commonly employed for research purpose are of the so-called **swimming-pool** design, where the **reactor core**, consisting of the fuel elements and the control rods, is situated in an open water pool. The water acts at the same time as moderator, refrigerant and radiation shield. Neutrons are extracted from the pool by means of tubes, known as **"glove fingers"**, which are

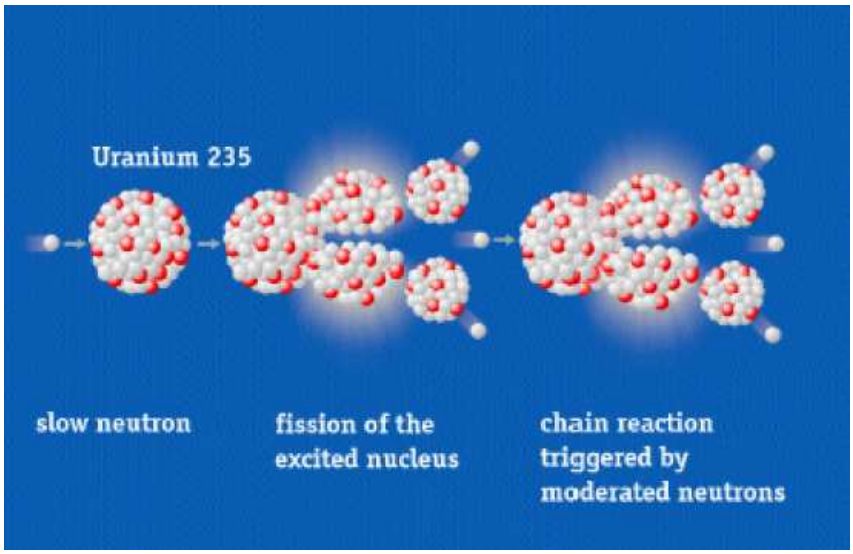

Figure 13: A schematic representation of the fission nuclear reaction.

tangential to the core. In some cases additional sources ("cold source", "hot source") are placed in the swimming pool to modify the neutron spectrum (see below). It is easy to understand that the neutron flux is maximised by a **compact core** design. To achieve this, top research reactors, such as the Institut Laue-Langevin (ILL) in Grenoble generally employ **highly-enriched uranium**, although low-enrichment designs are preferred for non-proliferation purposes and are actively researched.

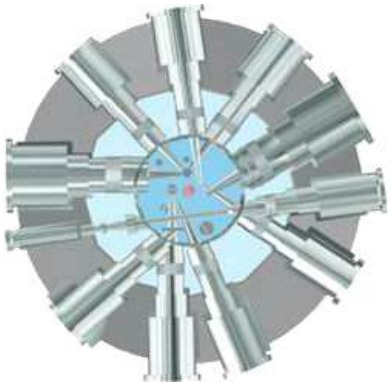

Figure 14: Horizontal section through the reactor pool (internal diameter approx. 5m) of the FRM-II research reactor in Munich — one of the most modern reactors worldwide. The larger "swimming pool" is filled with light water, whereas the pool close to the core contains heavy water. The tangential "glove fingers" of the neutron beam tubes — some pointing at the "hot" and "cold" sources — are clearly visible.

The most powerful reactor source in the world is the ILL. It generates fluxes of 1.5×10^{15} neutrons per second per cm^2 at the exit of the beam tubes, with a thermal power of 58.3 MW.

5.4.1 Neutron spectrum from a reactor source

A reactor source usually produces a **continuous** flux of neutrons (a remarkable exception is the IBR-2 fast pulsed reactor in Dubna, Russia — a truly remarkable design!). The **neutron spectrum** of the neutrons in the "swimming pool" is essentially a **Maxwell-Boltzman distribution centered at room temperature**, with a high-energy tail due to a residue of the fission neutrons and partially moderated neutrons. **Monochromatic neutron beams** can be produced by means of a **single-crystal monochromator** — naturally, suffering a very large reduction in neutron flux. These **thermal neutrons** are ideal for many neutron scattering applications, but sometimes is is useful to have a higher flux of slower (**cold**) of faster (**hot**) neutrons. For this purpose, special **cold and hot sources** are positioned in the reactor pool, with some of the beam tubes looking directly at them. Cold sources are typically liquid deuterium at $\sim$ 25 K. Hot sources are graphite blocks heated by the neutron themselves to around 900°C.

5.5 Spallation sources

When a fast particle, such as a high-energy proton, bombards a heavy atomic nucleus (such as lead, tungsten or tantalum), some neutrons are "spalled," or knocked out, in a nuclear reaction called spallation. Other neutrons are "boiled off" as the bombarded nucleus heats up, while the fast neutron produce secondary spallation reactions with other nuclei (fig 15). These reactions are much more efficient than fission at producing neutrons (20-30 neutrons are produced for each spallation event), but, of course, one has to accelerate the protons in the first place to energies of the order of to 0.5-2 GeV, using a linear accelerator (LINAC), a synchrotron or a combination thereof.

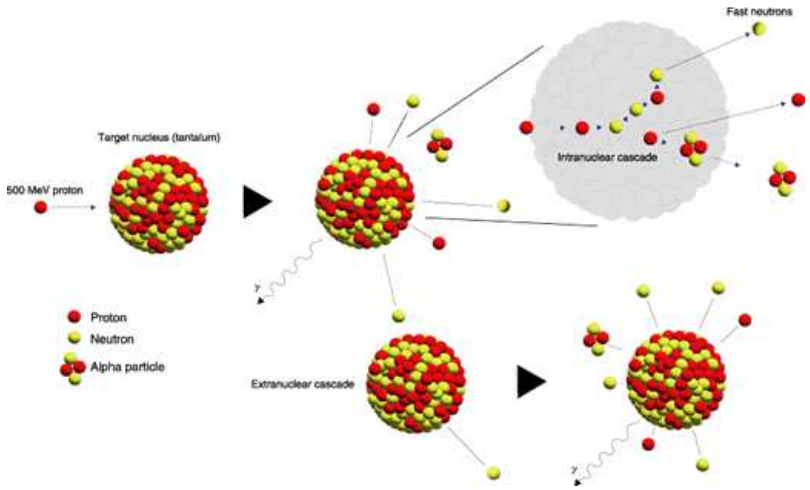

Figure 15: Schematic representation of some of the nuclear processes involved in "spallation" neutron production. Heavy-element nuclei are fragmented ("spalled") either by the incident protons (**top**) or by secondary neutrons (**bottom left**). Other nuclei are left in a highly excited state and "boil off" additional neutrons (**bottom right**).

The neutrons leaving the heavy-metal target are highly energetic, and need to be moderated before they can be employed for scattering experiments. This is done in a series of **moderators** that surround the **target assembly** (which usually includes a series of beryllium neutron reflectors as well). As for the case of reactor sources, **moderators can be held at different temperatures** to produce characteristic spectral distributions.

5.5.1 Continuous vs. pulsed spallation sources

The neutron flux from a spallation sources can be either **continuous** or **pulsed**, depending on the characteristic of the accelerator. Although successful **continuous spallation sources** have been built (for example, the SinQ neutron source at the Paul-Scherrer Institut in Villigen, near Zurich, Switzerland), the preferred design is that of a **pulsed spallation source**. In fact whereas the *average* neutron flux from a spallation source is 2-3 order of magnitude *smaller* than for a reactor, **the instantaneous neutron flux of a pulsed spallation source can be as high or higher than that of a reactor.**

In a pulsed spallation source, neutron of all energies are produced *at the same time* within a few μsec (after moderation), and with a *repetition rate* of 10-60 Hz. The wavelength of the neutrons can therefore be determined using the *time-of-flight* method, i.e., by measuring the time elapsed between the pulse and the neutron detection. This *removes the need of a monochromator* for most applications.

5.5.2 Characteristics of a pulsed spallation source

A modern pulsed spallation source, such as the ISIS facility in Chilton, Oxfordshire (fig. 16), comprises the following main components.

- **The proton accelerator system**. For ISIS, this consists of an ion source, a LINAC and a rapid-cycling synchrotron. Proton pulsed from the LINAC are "stored" and accelerated in the synchrotron to 800 MeV. Every 20 msec, a "septum" magnet in the synchrotron is excited, redirecting pulses of protons of a few nsec in length to either of the two targets.
- **The target-moderator assembly**. The heavy-metal target (tungsten or tantalum) is located at the centre of a beryllium reflector and is surrounded by **moderators** (water, liquid hydrogen or methane, solid methane). The moderators have to be relatively thin to preserve a tight pulse structure. The whole assembly is contained in a heavy concrete/steel block (the "monolith"), providing the radiation shielding.
- **The beamlines** look directly at the moderator surfaces. They can be simple collimating tubes or complex **neutron guides**, which work with the same principle of an optical fibre.
- **The instruments** (spectrometers, diffractometers etc.) include a **detector array**, connected with an electronic counting chain that can record the time of arrival of each neutron and is synchronized with the proton pulse on the target. The wavelength of the neutrons can therefore be determined by the Time-of-Flight method.

5.6 Neutron detectors

Essentially all types of X-ray detectors can be used to detect neutrons, provided that they are coupled with a suitable **neutron converter**, i.e., an element that capture neutrons and produces ionisation. **The energy released in the neutron capture process (several MeV) is much larger than the kinetic energy of the neutron (a few meV)**. Therefore, it has so far proven impossible to build an energy dispersive (or even discriminating) neutron detector. On the other hand, pulse-height analysis is used to discriminate neutron from γ events in the detector.

A neutron detector should be **efficient**, **fast** and **insensitive** to γ radiation. The most common types of neutron detectors are:

- ^3He **tubes**. It is essentially a proportional ion chamber filled with several bars of ^3He, which capture neutrons following the reaction in eq. 34. The proton and the triton are responsible for the ionisation, which is detected by the chamber. Area detectors can be built as either position-sensitive arrays of tubes or ^3He **2-dimensional wire detectors**.
- **Neutron scintillators**, employ scintillator glass or crystals doped with ^6Li, either enriched or

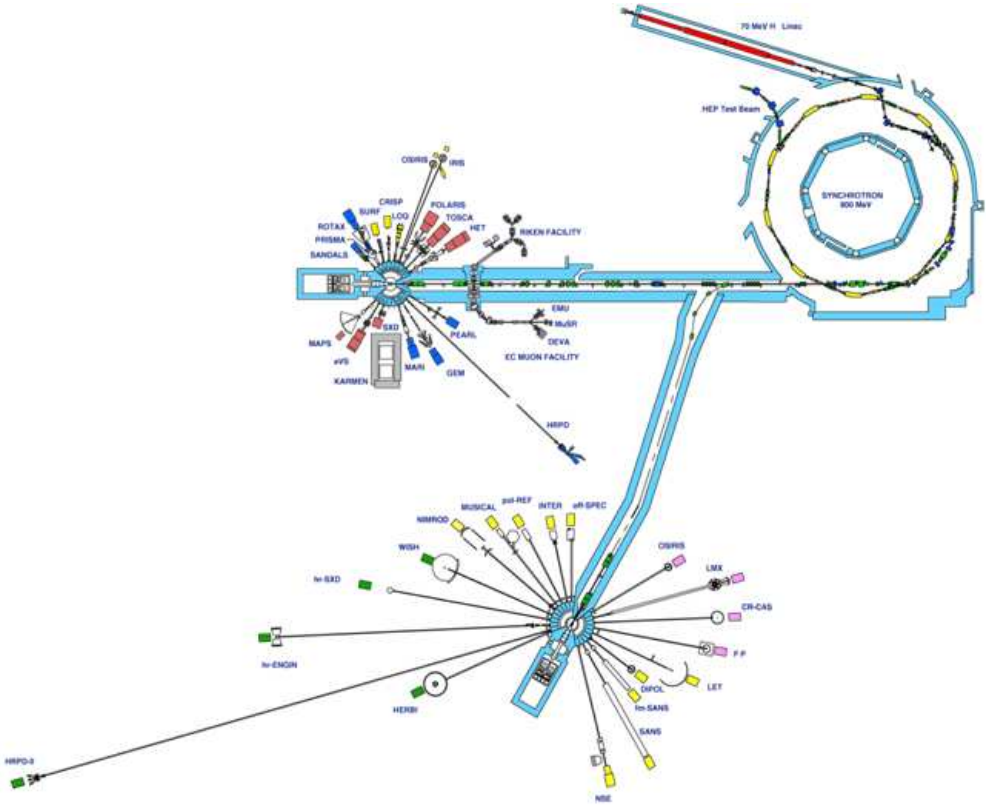

Figure 16: Schematic representation of the ISIS pulsed spallation neutron source, located in Chilton, Oxfordshire (near Harwell). One can recognise the **LINAC** (topmost), the **synchrotron** (top right) and the two **target stations** (left and bottom), surrounded by a series of **beamlines**.

in its natural abundance (7.5%). The scintillation event is triggered by the Li n-capture reactions, as shown in 34. Scintillators can be tessellated in intricate shapes, or used to build area detectors.

6 Appendix I: Beyond the free electron approximation

6.1 Resonant scattering and anomalous corrections to the form factor

Here, we repeat essentially the same derivation that led to the calculation of the Thomson cross section, but replacing the "free-electron" acceleration in eq. 4 with an expression appropriate to a **damped oscillator**.

$$m\left[\ddot{x} + \gamma\dot{x} + \omega_i^2 x\right] = (-e)\mathbf{E}(t) \tag{41}$$

$$\mathbf{a}(t) = \frac{(-e)}{m}\boldsymbol{\epsilon}E_0 e^{-i\omega t}\,\frac{\omega^2}{\omega^2 - \omega_i^2 + i\omega\gamma_i} \tag{42}$$

where ω_i is the resonance frequency of each electron. If we use 42 instead of 4 in the previous derivations, we obtain in general a **complex scattering amplitude**. It is easy to evaluate this in the case $\omega \gg \omega_i$, i.e., for example, for scattering of high-energy X-rays ($> 20KeV$) from first-period transition-metal ions. In this case

$$f(\mathbf{q}) = \sum_i [f(\mathbf{q})_{Thom}]_i \left(1 - \frac{\omega_i^2}{\omega^2} + i\frac{\gamma_i}{\omega}\right) \tag{43}$$

6.2 Compton scattering

One important issue related to the bound nature of electrons is the fact that no elastic scattering is possible for a truly free electron, but the Compton formula applies instead:

$$\frac{k'}{k} = \frac{1}{1 + \frac{\hbar\omega}{mc^2}(1 - \cos\gamma)} \tag{44}$$

At low photon energy, the photon momentum is transferred to the atom as a whole (much heavier) or to the entire crystal, and the scattering is elastic to a very good approximation. As the energy increases nearing the rest mass energy of the electron ($mc^2 = 511$ KeV), the Compton scattering cross section increases.

7 Appendix II: Scattering of particle beams

As we have seen in the previous sections (eq. 8), a plane wave impinging on a quasi-free distribution of charges produces a *spherical* wave, the amplitude of which is proportional to the incident amplitude E_0. The coefficient multiplying the spherical wave is

$$r_0\, f(\mathbf{q})\, [\cos\xi\, \boldsymbol{\epsilon}'_\sigma + \sin\xi\, \cos\gamma\, \boldsymbol{\epsilon}'_\pi] \tag{45}$$

can be complex. In the general case, for a given wavelength, this coefficient depends on both angular variables of the scattered beam, but for spherically-symmetric atoms it depends only on the scattering angle $\gamma = 2\theta$. Importantly, **the cross section is equal to the square modulus of the spherical wave coefficient**. As we shall see shortly, the same principles applies to the scattering of particle beams, provided that the particle beam is described quantum-mechanically, so that the wave-like nature of the particles is apparent. Indeed, quantum mechanics is essential to obtain exact results, although the essential features are often classical or semi-classical in origin. In addition, it is often convenient to discuss the *stationary* problem rather than the time-dependent problem of a single particle starting off far away from the scatterer. The stationary problem is equivalent to considering a steady streams of particle coming from infinity, which is partly converted into a current of scattered particles in the form of a spherical wave. Finally, provided that we operate in the non-relativistic limit, we can consider the 2-particle scattering problem to be equivalent to that of scattering from a static potential $V(\mathbf{r})$, provided that the mass of the particle is replaced by the effective mass

$$m_{eff} = \frac{m_1\, m_2}{m_1 + m_2} \tag{46}$$

Hereafter, we will simply refer at the effective mass as m.

7.1 Wavefunction equation for the static scattering problem

We are looking for the solutions $\psi(\mathbf{r})$ for the following eigenfunction equation

$$\left(-\frac{\hbar^2}{2m}\nabla^2 + V(\mathbf{r})\right)\psi(\mathbf{r}) = E\psi(\mathbf{r}) \tag{47}$$

For the scattering problem, we are not interested in the bound states, so we will focus on the continuous spectrum with positive eigenvalues. We also expect that, at long distances from the

origin of the potential, the solution will approximate a plane wave (at least on one side), with energy $E = \frac{\hbar^2 k^2}{2m}$. By defining the new potential $U(\mathbf{r}) = \frac{2m}{\hbar^2} V(\mathbf{r})$ we arrive at the equation:

$$\left(\nabla^2 + k^2\right) \psi(\mathbf{r}) = U(\mathbf{r})\psi(\mathbf{r}) \tag{48}$$

The solution of eq: 48 with the right side set to zero is clearly a plane wave

$$\varphi(\mathbf{r}) = e^{i\mathbf{k}\cdot\mathbf{r}} \tag{49}$$

Eq. 49 represent the free-particle limit of the wavefunction, i.e., the **incident** wave. Therefore, we will later employ 49 with $\mathbf{k} = \mathbf{k}_i$.

An important step towards the solution of the general eq. 48 is to solve the point-source equation:

$$\left(\nabla^2 + k^2\right) \psi(\mathbf{r}) = \delta(\mathbf{r}) \tag{50}$$

The solutions of equations of the type 50 are known as **Green's functions**. It can be shown rather straightforwardly that the following two functions are solutions of eq: 50

$$\begin{aligned} G^+(\mathbf{r}) &= -\frac{1}{4\pi}\frac{e^{ik|\mathbf{r}|}}{|\mathbf{r}|} \\ G^-(\mathbf{r}) &= -\frac{1}{4\pi}\frac{e^{-ik|\mathbf{r}|}}{|\mathbf{r}|} \end{aligned} \tag{51}$$

To verify that 51 are indeed solutions of eq: 50 it is sufficient to use the relation

$$\nabla^2(ab) = a\nabla^2 b + b\nabla^2 a + 2\boldsymbol{\nabla} a \cdot \boldsymbol{\nabla} b \tag{52}$$

The two solutions in eq. 51 are expanding and contracting spherical waves, respectively. By selecting the former, we can rewrite eq. 48 in an *integral* form (we only write the solution with the expanding Green function):

$$\psi(\mathbf{r}) = \varphi(\mathbf{r}) + \int d\mathbf{r}' G^+(\mathbf{r} - \mathbf{r}') U(\mathbf{r}')\psi(\mathbf{r}') \tag{53}$$

Since we are primarily interested in solutions far away from the region where the potential is non-zero, we can employ a far-field approximation similar to that of eq: 16. The key observation here

is that **$\mathbf{r}'$ is small, because the potential is non-zero only near the scatterer**. Also, importantly, $|\mathbf{k}_i| = |\mathbf{k}_f| = k$, since we are dealing with **elastic scattering**. The correspondence between eq. 16 and eq. 54 is clear if we write $\mathbf{k}_f = k\mathbf{n}$

$$k|\mathbf{r} - \mathbf{r}'| \approx kr - \mathbf{k}_f \cdot \mathbf{r}' \tag{54}$$

after some simple algebra we obtain (again, at long distances from the scattering centre):

$$\psi(\mathbf{r}) = e^{i\mathbf{k}\cdot\mathbf{r}} + \left[-\frac{1}{4\pi}\int d\mathbf{r}'\, e^{-i\mathbf{k}_f\cdot\mathbf{r}'} U(\mathbf{r}')\psi(\mathbf{r}')\right]\frac{e^{ikr}}{r} \tag{55}$$

Eq. 55 has a very pleasing form: it is very similar to eq. 8, and we could surmise that the squared modulus of the expression in square brackets (the "scattering amplitude") is the cross section (this is proven in most standard quantum mechanics textbooks by introducing the probability current density). Here, we will take it for granted without further proof. Unfortunately, the scattering amplitude in eq. 55 depends on the wavefunction itself. We can make progress by assuming that potential is in some sense "small", so that the spherical wave is a small component of the overall wavefunction. We can therefore attempt to expand the integral term in series:

$$\begin{aligned}-\frac{1}{4\pi}\int d\mathbf{r}'\, e^{-i\mathbf{k}_f\cdot\mathbf{r}'} U(\mathbf{r}')\psi(\mathbf{r}') \approx \\ -\frac{1}{4\pi}\int d\mathbf{r}'\, e^{-i\mathbf{k}_f\cdot\mathbf{r}'} U(\mathbf{r}')\varphi(\mathbf{r}') + \left(\frac{1}{4\pi}\right)^2 \int d\mathbf{r}d\mathbf{r}'\varphi(\mathbf{r}')\frac{e^{ik|\mathbf{r}-\mathbf{r}'|}}{|\mathbf{r}-\mathbf{r}'|}U(\mathbf{r})U(\mathbf{r}') + ...\end{aligned} \tag{56}$$

The series in eq. 56 is known as the **Born series**; taking the first term alone is know as the **first Born approximation**. It is easy to obtain the expression for the scattering cross section in the first Born approximation; remembering that $\varphi(\mathbf{r}')$ is the plane wave $exp(i\mathbf{k}_i \cdot \mathbf{r}')$, we obtain:

$$\left(\frac{d\sigma}{d\Omega}\right)_{Born} = \left|\frac{1}{4\pi}\int d\mathbf{r} e^{-i\mathbf{q}\cdot\mathbf{r}} U(\mathbf{r})\right|^2 \tag{57}$$

where $\mathbf{q} = \mathbf{k}_f - \mathbf{k}_i$. In other words, **in the first Born approximation, the cross section is proportional to the Fourier transform of the potential energy**.

7.2 Elastic scattering of electrons in the 1^{st} Born approximation

As a first example of scattering of a particle beam, we will consider the elastic scattering of electrons from the Coulomb potential produced by the nucleus and by the electrons bound in an

atom. For simplicity, we will consider electrons as spinless particles. Based on eq. 57, we need to calculate the *potential*, and for this is useful to recall that

$$\nabla^2 e^{-i\mathbf{q}\cdot\mathbf{r}} = -q^2 e^{-i\mathbf{q}\cdot\mathbf{r}} \tag{58}$$

Recalling that $U(\mathbf{r}) = \frac{2m}{\hbar^2}V(\mathbf{r})$, we can rewrite the integral in eq. 57 as

$$\frac{1}{4\pi}\int d\mathbf{r} e^{-i\mathbf{q}\cdot\mathbf{r}} U(\mathbf{r}) = -\frac{m}{2\pi q^2\hbar^2}\int d\mathbf{r} V(\mathbf{r})\nabla^2 e^{-i\mathbf{q}\cdot\mathbf{r}} = -\frac{m}{2\pi q^2\hbar^2}\int d\mathbf{r} e^{-i\mathbf{q}\cdot\mathbf{r}}\nabla^2 V(\mathbf{r}) \tag{59}$$

where the rightmost expression is obtained by integrating twice by part and assuming that both the potential and its first derivative are zero at infinite distance from the origin. We can now use Poisson's equation and the expression for the charge density of an atom of atomic number Z:

$$\nabla^2\Phi = \frac{\rho}{\epsilon_0} \tag{60}$$

$$V = (-e)\Phi \tag{61}$$

$$\rho(\mathbf{r}) = Ze\delta(\mathbf{r}) + (-e)\rho_{el}(\mathbf{r}) \tag{62}$$

where Φ is here the electrostatic potential and $\rho_{el}(\mathbf{r})$ is the same electron density we have employed for X-rays. To find the expression for the elastic scattering cross section:

$$\frac{d\sigma}{d\Omega} = \left(\frac{e^2}{\epsilon_0}\frac{m}{2\pi q^2\hbar^2}\right)^2 \left|Z - \int d\mathbf{r} e^{-i\mathbf{q}\cdot\mathbf{r}}\rho_{el}(\mathbf{r})\right|^2 \tag{63}$$

We can see the immediate analogy with the scattering cross section for X-rays (eq. 23). The integral term is exactly the same as the X-ray form factor, and is referred to as f_X in the text. The term in brackets takes the place of the classical electron radius, and is numerically

$$\frac{e^2}{\epsilon_0}\frac{m}{2\pi\hbar^2} = 3.38\times10^{-10}\ \text{m Å}^{-2} \tag{64}$$

whereas, for comparison, the classical electron radius is $r_0 = \dfrac{e^2}{4\pi\epsilon_0 mc^2} = 2.82\times10^{-15}\,\text{m}$. We can see therefore that for all typical values of q (1–10 Å^{-1}) employed for electron diffraction experiments, **the scattering amplitudes for electrons is much larger than for X-rays**.

The elastic scattering amplitude for electrons f^B is often expressed in wavelength/angle units as in eq. 65. One can find tabulated values for neutral and ionised atoms in the International Tables for Crystallography, volume C [1], p 263 (λ is the electron wavelength and both λ and f^B in eq. 65 are expressed in Å):.

$$f^B(\sin\theta/\lambda) = 0.023934\lambda^2[Z - f_X(\sin\theta/\lambda)]/\sin^2\theta \tag{65}$$

7.3 Nuclear scattering of "slow" neutrons

By looking at tab. 2, it is immediately apparent that the kinetic energies of neutrons employed is typical scattering experiments is much lower than the energies of nuclear reactions, which are typically in the MeV range. In fact, it is established from nuclear physics that the neutron-nuclear interaction can be approximated with a square potential well of depth $V_0 \approx 50$ MeV and range $d = 1.3A^{\frac{1}{3}} \times 10^{-15}$ m, where A is the mass number of the nucleus. It is therefore implausible that the first Born approximation could be applied as such to the scattering of slow neutrons. In fact, a more detailed calculation shows that the first Born approximation is applicable only to neutrons with $E > 25$ MeV.

Nevertheless, Fermi proposed in 1936 that slow neutron scattering could still be satisfactorily treated in the first Born approximation. The general idea here is that the wavelength of the neutrons is so large that one can replace the real potential with a "pseudopotential" (known as the Fermi pesudopotential), which yields the same first Born scattering amplitude and for which the approximation definitely applies. For this, one observes that, over the range of the true potential, the phase of the neutron is essentially constant in eq. 56, and the scattering amplitude can be written as:

$$f = -\frac{m}{2\pi\hbar^2}\int d\mathbf{r}V_0(\mathbf{r}) = -\frac{m}{2\pi\hbar^2}V_0 d^3 \tag{66}$$

We could therefore think of decreasing the depth of the potential well into the thermal ranges by increasing the range of the potential by a factor of, ~ 100, while maintaining the same value of the scattering amplitude and, crucially, still keeping the range much smaller than the neutron wavelength — a set of conditions for which the first Born approximation definitely applies. This conjecture led to the development of the **Fermi pseudopotential**, which has the form:

$$V_F(\mathbf{r}) = \frac{2\pi\hbar^2}{m}b_F\delta(\mathbf{r}) \tag{67}$$

where b_F is the scattering length, known as the **Fermi length**. In practice, the Fermi pseu-

dopotential is completely satisfactory to describe nuclear neutron scattering for diffraction experiments, and only need corrections (analogous to the X-ray anomalous corrections) only for energies near neutron-nuclear resonances.

Here are some important facts about neutron scattering lengths and cross sections:

- Neutron scattering amplitudes **do not depend on q**, i.e., they carry no form factor. For diffraction experiment this is crucially important, because it means that the intensity of the diffraction features **does not decay at high angles as fast as in the case of X-rays** (we will see in the next lecture that thermal motion causes high-q Bragg intensity decay even in the case of neutrons). They are also largely independent on the neutron energy, at least in the regime of interest for neutron diffraction.

- Fermi lengths for typical nuclei are of the order of a few fm (10^{-15} m), which means that they are comparable to the classical electron radius. However, atoms have a single nucleus and many electrons, so X-ray scattering cross sections in the *forward* direction are typically much larger than neutron cross sections. Neutron cross sections are traditionally measured in **barns** (10^{-28} m^2).

- **Neutron absorption is also much lower than for X-rays**, which, together with the previous observation, means that attenuation (absorption + scattering) lengths are of the order of **cm for neutrons** and of μ**m for X-rays**. This has a profound effect on the design of diffraction experiments exploiting the two types of radiation.

- Fermi lengths vary across the periodic table without any particular regularity. They can be positive or negative depending on the sign of the nuclear potential. They depend on the *isotope*, often very strongly, and also on the direction of the *nuclear spin* with respect to the *neutron spin*. This has two main consequences, one "positive" and one "negative": the "negative" consequence is the presence of "incoherent" scattering, due to the random mixture of different isotope and spin orientations, which contributes to the experimental background. The "positive" consequence is the possibility to exploit different isotopes of the same element to gain additional contrast.

7.4 The Fermi golden rule and its connection with the first Born approximation

In the previous sections, we have considered the Born series for a spinless particle beam, so that there was no internal degree of freedom to consider. In addition, the internal state of the scatterer (in our case a time-independent potential) was also unchanged during the collision. Consequently, the energy of the scattered particle remains the same after the collision. It is

useful to extend our description of the scattering to cases in which there are internal degrees of freedom which may be altered in the collision. The Fermi golden rule (the development of which is mainly due to Dirac) is widely employed to calculate the transition probability of an eigenstate (in our case, a plane wave), into a continuum of "final" states due to a perturbation. As in the case of the first Born approximation, it is the first term of a perturbative expansion, and is applicable within very similar conditions to the first Born approximation, namely that the final states do not significantly deplete the original eigenstate. Here, we only quote the general result for the scattering cross section between states with wavevectors $\mathbf{k}_i$ and $\mathbf{k}_f$ and an internal transition between states λ_i and λ_f with energies E_i and E_f, respectively.

$$\frac{d\sigma}{d\Omega dE_f} = \frac{k_f}{k_i} \left| (m/2\pi\hbar^2) \langle \mathbf{k}_f, \lambda_f \left| \hat{V} \right| \mathbf{k}_i, \lambda_i \rangle \right|^2 \delta(\hbar\omega + E_i - E_f) \tag{68}$$

where we have employed the familiar $\langle bra| - |ket\rangle$ notation, $V(\mathbf{r})$ is the "perturbing" potential and $\hbar\omega = \hbar^2(k_f^2 - k_i^2)/2m$, ensuring energy conservation.

It is a simple exercise to show that, for elastic scattering in the absence of internal degrees of freedom, the "golden rule" cross section in eq. 68 is exactly the same as the first Born approximation result in eq. 57.

7.5 Magnetic scattering of neutrons

We will exemplify the application of the Fermi golden rule by outlining the calculation of the scattering of slow neutron onto a magnetic atom. We will assume that no energy is exchanged in the process. Here, the interaction potential is naturally the dipole interaction between the neutron spin $\mathbf{S}$ and the magnetic field $\mathbf{B}(\mathbf{r})$ generated by the electrons(we will assume zero external magnetic field for simplicity). When dealing with **elastic** magnetic scattering, the initial and final states of the **atoms** are assumed to be the *same*, implying that conservation of linear and angular momenta is ensured by the crystal as a whole. Therefore, the **operator** quantities (here indicated explicitly with a "$\hat{}$") are **only those acting on the *neutron* coordinates**.

$$V(\mathbf{r}) = -\gamma_N \mu_N \hat{\mathbf{S}} \cdot \mathbf{B}(\mathbf{r}) \text{ [Joules]} \tag{69}$$

where $\hat{\mathbf{S}}$ is the **neutron spin operator**, γ_N is the neutron gyromagnetic ratio (-1.9130418) and μ_N is the nuclear magneton ($\frac{e\hbar}{2m_p} = 5.05078324(13) \times 10^{-27}$ JT^{-1}). The magnetic field of a single electron moving with velocity $\mathbf{v}$ is

$$\mathbf{B}(\mathbf{r}) = \boldsymbol{\nabla} \times \left[\frac{\mu_0}{4\pi} \frac{\boldsymbol{\mu}_e \times \hat{\mathbf{r}}}{r^3} \right] + \frac{-e\mu_0}{4\pi} \frac{\hat{\mathbf{v}} \times \hat{\mathbf{r}}}{r^3} \tag{70}$$

Where $\boldsymbol{\mu}_e$ is the magnetic moment of the electron, given by (μ_B is the Bohr magneton, $\mathbf{s}$ is the spin of the electron)

$$\boldsymbol{\mu}_e = -2\mu_B \mathbf{s} \tag{71}$$

The two terms in eq. 70 represent the *spin* and *orbital* part of magnetic moment. The "hatted" vector quantities in eq. 70 are meant as operators (so, for instance,

$$\hat{\mathbf{v}} = -i\hbar\boldsymbol{\nabla} \tag{72}$$

The derivation of the cross section in in eq. 68, even in the general case of inelastic scattering and is quite straightforward, and is reported, for example, in [2]. Here, for simplicity, we only report the final result for *elastic scattering of unpolarised neutrons, i.e., we are averaging on the initial and final neutron spins*:

$$\frac{d\sigma}{d\Omega} = \gamma_N^2 r_0^2 \mathbf{Q}_\perp^\dagger \cdot \mathbf{Q}_\perp \tag{73}$$

where

- r_0 is the **classical electron radius**. This means that *the scattering amplitude for a neutron by the magnetic field of a single electron is comparable to the Thomson scattering amplitude of X-rays*.
- $\mathbf{Q}$ is given by the formula (*spin only scattering*)

$$\mathbf{Q} = \sum_i e^{i\mathbf{q}\cdot\mathbf{r}_i}\mathbf{s}_i \tag{74}$$

  and, in the general case, is **the Fourier transform of the magnetisation density (spin + orbital) for unpaired electrons**. In simple cases,

$$\mathbf{Q} = f_m(q)\boldsymbol{\mu} \tag{75}$$

  $\boldsymbol{\mu}$ is the magnetic moment of the atom and and $f_m(q)$ — the *magnetic form factor* — takes the place of the X-ray form factor in the analogous expression for Thomson scattering.

- $\mathbf{Q}_\perp$ is the projection of $\mathbf{Q}$ *perpendicular* to the scattering vector $\mathbf{q}$

$$\mathbf{Q}_\perp = \frac{1}{q^2}\mathbf{q} \times \mathbf{Q} \times \mathbf{q} \tag{76}$$

in practical terms, this means that **neutrons are only sensitive to the components of the magnetic moments *perpendicular* to the scattering vector.**

- If we take into account the direction of the neutron spins, the cross section will contain terms of the kind $\hat{\mathbf{S}} \cdot \mathbf{Q}_\perp$ and depends on the initial and final states of the neutron. **For pure magnetic elastic scattering, the cross section is non-zero only for *opposite* incident and scattered neutron spins — we say that it is "spin flip" only**.

8 Useful constants

$$
\begin{aligned}
\epsilon_0 &= 8.854187 \times 10^{-12} \text{ F m}^{-1} \text{ — vacuum permittivity} \\
\mu_0 &= 4\pi \times 10^{-7} \text{ N } A^{-2} \text{ — vacuum permeability (exact)} \\
c &= 2.99792458 \times 10^{8} \text{ m } s^{-1} \text{ — speed of light in vacuum} \\
e &= 1.602176487(40) \times 10^{-19} \text{ C — unit charge}
\end{aligned}
$$

$$
\begin{aligned}
m_e &= 9.10938215(45) \times 10^{-31} \text{ Kg — electron rest mass} \\
m_p &= 1.672621637(83) \times 10^{-27} \text{ Kg — proton rest mass} \\
m_n &= 1.674927729(28) \times 10^{-27} \text{ Kg — neutron rest mass}
\end{aligned}
$$

$$
\begin{aligned}
r_0 &= \frac{e^2}{4\pi\epsilon_0 m c^2} = 2.82 \times 10^{-15} \text{ m — classical electron radius} \\
\mu_N &= \frac{e\hbar}{2m_p} = 5.05078324(13) \times 10^{-27} \text{ JT}^{-1} \text{ — nuclear magneton} \\
\gamma_N &= -1.9130418 \text{ — neutron gyromagnetic ratio} \\
\mu_B &= \frac{e\hbar}{2m_e} = 9.27400915(23) \times 10^{-24} \text{ JT}^{-1} \text{ — Bohr magneton}
\end{aligned}
$$

9 Bibliography

The International Tables for Crystallography vol C [1] contains an excellent compendium of most X-ray, neutron and electron diffraction techniques.

J.D. Jackson, "Classical Electrodynamics" [3]. I have follow this book for the derivation of the classical X-ray scattering cross section. It is a very complete compendium of electrodynamics, although not always easy to digest...

A.S. Davydov, "Quantum Mechanics" [4]. I followed this rather old quantum mechanics textbook (mainly for sentimental reasons) for the calculation of the cross sections in the first Born approximation (Appendix II).

References

[1] T. Hahn, ed., *International tables for crystallography*, vol. C (Kluver Academic Publisher, Do- drecht: Holland/Boston: USA/ London: UK, 2002), 5th ed.

[2] Stephen W. Lovesey, "Theory of neutron scattering from condensed matter", Oxford Science Publications, Clarendon Press, Oxford (1984) — Volume 2.

[3] John D. Jackson, "Classical Electrodynamics", John Wiley & sons, New York, Chichister, Brisbane, Toronto, Singapore, (1975)

[4] A.S. Davydov, "Quantum Mechanics", Pergamon/Addison-Wesley, (1965).